

Ellipsometric study of polycrystalline silicon films prepared by low-pressure chemical vapor deposition

P. Petrik,^{a)} T. Lohner, M. Fried, L. P. Biró, N. Q. Khánh, and J. Gyulai
MTA-MFA, Research Institute for Technical Physics and Materials Science, H-1121 Budapest, Konkoly Thege u. 29-33., Hungary

W. Lehnert and C. Schneider
Fraunhofer Institut für Integrierte Schaltungen, Schottkystrasse 10, D-91058 Erlangen, Germany

H. Ryszel
Fraunhofer Institut für Integrierte Schaltungen, Schottkystrasse 10, D-91058 Erlangen, Germany, and Lehrstuhl für Elektronische Bauelemente, Friedrich-Alexander Universität Erlangen-Nürnberg, Cauerstrasse 6, D-91058 Erlangen, Germany

(Received 22 April 1999; accepted for publication 27 October 1999)

Polysilicon layers with thicknesses between 8 and 600 nm deposited by low-pressure chemical vapor deposition at temperatures ranging from 560 to 640 °C were characterized by spectroscopic ellipsometry (SE) to determine the layer thicknesses and compositions using multilayer optical models and the Bruggeman effective-medium approximation. The dependence of the structural parameters on the layer thickness and deposition temperature have been investigated. A better characterization of the polysilicon layer is achieved by using the reference data of fine-grained polysilicon in the optical model. The amount of voids in the polysilicon layer was independently measured by Rutherford backscattering spectrometry (RBS). The SE and RBS results show a good correlation. The comparison of the surface roughness measured by SE and atomic force microscopy (AFM) shows that independently of the AFM window sizes, a good correlation of the roughness determined by SE and AFM was obtained. © 2000 American Institute of Physics. [S0021-8979(00)01604-2]

I. INTRODUCTION

Polycrystalline silicon (*pc*-Si) films deposited by low-pressure chemical vapor deposition (LPCVD) have been intensively studied because of their application to microelectronics as gate material for field-effect transistors, as emitter in bipolar transistors, and as parts of interconnects. Thin-film transistors fabricated in polysilicon have attracted considerable interest for large-area electronics and for the application to three-dimensional integrated circuits.^{1,2}

Studies on polysilicon have been performed by several authors. The temperature and pressure dependence of the mode of growth,³ texture and stability,⁴ crystal structure, electrical resistance, segregation at grain boundaries, oxidation rate, index of refraction, POCL₃ doping, oxidation, etch rate, and reflectivity as a function of the deposition temperature⁵ are some of the most important parameters.

Polysilicon has been studied intensively also by spectroscopic ellipsometry (SE). SE has proven to be very effective for the characterization of thin surface layers because it is fast, sensitive, precise, nondestructive, and it can be used for *in situ* measurements.⁶⁻⁹ A new approach to obtain more detailed information on the surface roughness is to do comparison of the ellipsometric results with data obtained from atomic force microscopy (AFM).¹⁰⁻¹²

One approach of determining the physical properties of polysilicon is to analyze its dielectric function in terms of

line shapes and fine structures in the vicinity of the critical points of interband transitions. Changes in the dielectric function can be attributed to heavy doping,¹³ to surface roughness or grain boundaries,^{14,15} to name the most important effects.

To measure the layer thickness, surface roughness, or microstructure of polysilicon using ellipsometry, *a priori* knowledge of the thin-film optical functions or a technique to calculate these values are needed. Optical properties of *pc*-Si influence considerably with its microstructure. To circumvent the influence of microstructure, the Bruggeman effective-medium approximation (B-EMA) is used to calculate the dielectric function of the layer assuming a mixture of materials with different dielectric functions determined independently.¹⁶ This method allows to characterize a material by multilayer structures,¹⁷⁻¹⁹ and to obtain all layer thicknesses and compositions.^{20,21} Layer inhomogeneity can be properly taken into account.²²⁻²⁴

LPCVD deposited polysilicon layers were modelled using the B-EMA by assuming them as a mixture of single-crystalline silicon (*c*-Si), LPCVD deposited amorphous silicon (*a*-Si) and voids.²⁵⁻²⁷ Jellison *et al.* have, however, shown that this standard technique for simulating the optical functions of fine-grained polycrystalline silicon does not fit the ellipsometry data.²⁸ This statement has been justified earlier. It was shown that using fine-grained *pc*-Si reference data in the optical model give better results and additional information on the layer structure.^{29,30}

^{a)}Electronic mail: petrik@mfa.kfki.hu

The aim of this work is to characterize the structure of polysilicon layers prepared at different deposition temperatures. The microstructural information obtained from the B-EMA was correlated with the layer thickness and the deposition temperature.

II. EXPERIMENT

Single-crystal, (111)-oriented, 15–20 Ω cm, *p*-type Czochralsky-silicon wafers with ≈100 nm thermal oxide were used as substrates for polysilicon deposition. Polysilicon layers were prepared using LPCVD at a pressure of 0.27 mbar and a gas flow of 100 sccm. The deposition temperatures were 600, 620, and 640 °C. Samples were also prepared under a pressure of 0.33 mbar and 50 sccm gas flow at temperatures of 560 and 580 °C.

SE measurements were carried out over the spectral range of 250–840 nm in 5 nm steps using a SOPRA ES4G spectroscopic ellipsometer choosing an angle of incidence of 75°.

SE provides $\tan \Psi$ and $\cos \Delta$ spectra, where Ψ and Δ are the ellipsometric angles which describe the reflection of the polarized light. Evaluation of the SE data was carried out using appropriate optical models. Calculated spectra are fitted to measured ones by varying the wavelength-independent model parameters using a linear regression analysis (LRA). The best fit model parameters are obtained in terms of their 95% confidence limits by minimizing the following unbiased estimator σ of the mean square deviation:

$$\sigma = \left[\frac{1}{(N-P-1)} \sum_{j=1}^N \{(\cos \Delta_j^{\text{meas}} - \cos \Delta_j^{\text{calc}})^2 + (\tan \Psi_j^{\text{meas}} - \tan \Psi_j^{\text{calc}})^2\} \right]^{1/2}, \quad (1)$$

where N is the number of independently measured values corresponding to different wavelengths and P is the number of unknown model parameters. (Here “meas” and “calc” refer to measured and calculated values, respectively.)

The density deficit measured by SE was crosschecked by Rutherford backscattering spectrometry (RBS) measurements. The analyzing beam was a 1.5 MeV $^4\text{He}^+$. The detector was placed to detect ions scattered through $\Theta=165^\circ$. The RBX code written by Kótai³¹ was used to evaluate the RBS spectra.

The AFM measurements were made by a Digital Instruments NanoScope Scanning Probe Microscope in tapping mode with scan window sizes of 1×1, 10×10, and 50×50 μm². Si tips with a resonant frequency of the cantilever of 300 kHz were used. Because the roughness values are influenced by tip, scan size, and scan conditions, the measurement parameters were kept identical from sample to sample. Images of 256×256 pixels were acquired at a scan rate of 3 Hz.

III. OPTICAL MODELS

The optical model for the sample deposited at $T_s = 560^\circ\text{C}$ consists of a buried oxide layer, an amorphous silicon layer, and a silicon dioxide layer (Model A in Fig. 1).

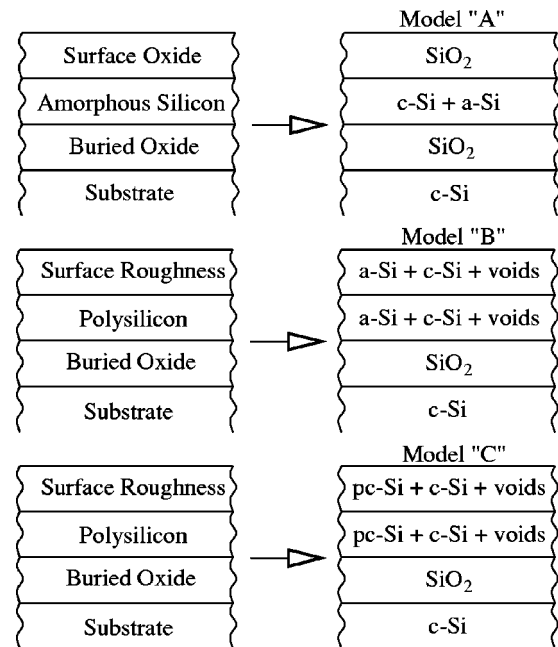


FIG. 1. Optical models for polysilicon-on-oxide structures. Model A can be used for samples deposited at 560 °C. Model B and Model C are used for deposition temperatures of 600–640 °C. Model B is the conventional method for describing polysilicon-on-oxide samples. In our case better results were obtained using Model C.

The surface roughness measured by AFM was 0.09 nm, and therefore, it was considered to be negligible. The measured and fitted ellipsometry spectra for $T_s = 560^\circ\text{C}$ are plotted at the top of Fig. 2. The agreement between the measured and fitted spectra is excellent in the whole spectral range ($\sigma = 0.02$). The LRA resulted in a surface oxide thickness of 1.2 ± 0.1 nm, an almost totally amorphous silicon layer (2.6% *c*-Si and $97.4 \pm 1.6\%$ *a*-Si) of 480.3 ± 1.7 nm, and in a buried oxide thickness of 112.7 ± 4.7 nm (see the insert in Fig. 2). The uncertainties of the model parameters are very low.

The layers in the optical model for the samples deposited at 600 °C and above represent the microscopic surface roughness, the polysilicon layer, and the buried oxide layer (Model B and C in Fig. 1). The dielectric function of the polysilicon layer can be obtained from EMA if the polysilicon layer can be assumed as a microscopically heterogeneous but macroscopically homogeneous material which consists of a random mixture of separate phases. Furthermore, the phases have to be large enough to preserve their individual dielectric functions but smaller than the wavelength of the measurement light. The relative compositions (volume fractions) of the separate regions are the obvious parameters describing such a material. Then, in the case of two components, the dielectric function $\bar{\epsilon}$ of the polysilicon layer can be expressed as

$$\frac{\bar{\epsilon} - \bar{\epsilon}_h}{\bar{\epsilon} + y\bar{\epsilon}_h} = f_a \frac{\bar{\epsilon}_a - \bar{\epsilon}_h}{\bar{\epsilon}_a + y\bar{\epsilon}_h} + f_b \frac{\bar{\epsilon}_b - \bar{\epsilon}_h}{\bar{\epsilon}_b + y\bar{\epsilon}_h}, \quad (2.1)$$

where $\bar{\epsilon}_h$ is the dielectric function of the host material, f_a and f_b are the volume fractions of the constituents ($f_a + f_b = 1$, if two components are present), $\bar{\epsilon}_a$ and $\bar{\epsilon}_b$ are the di-

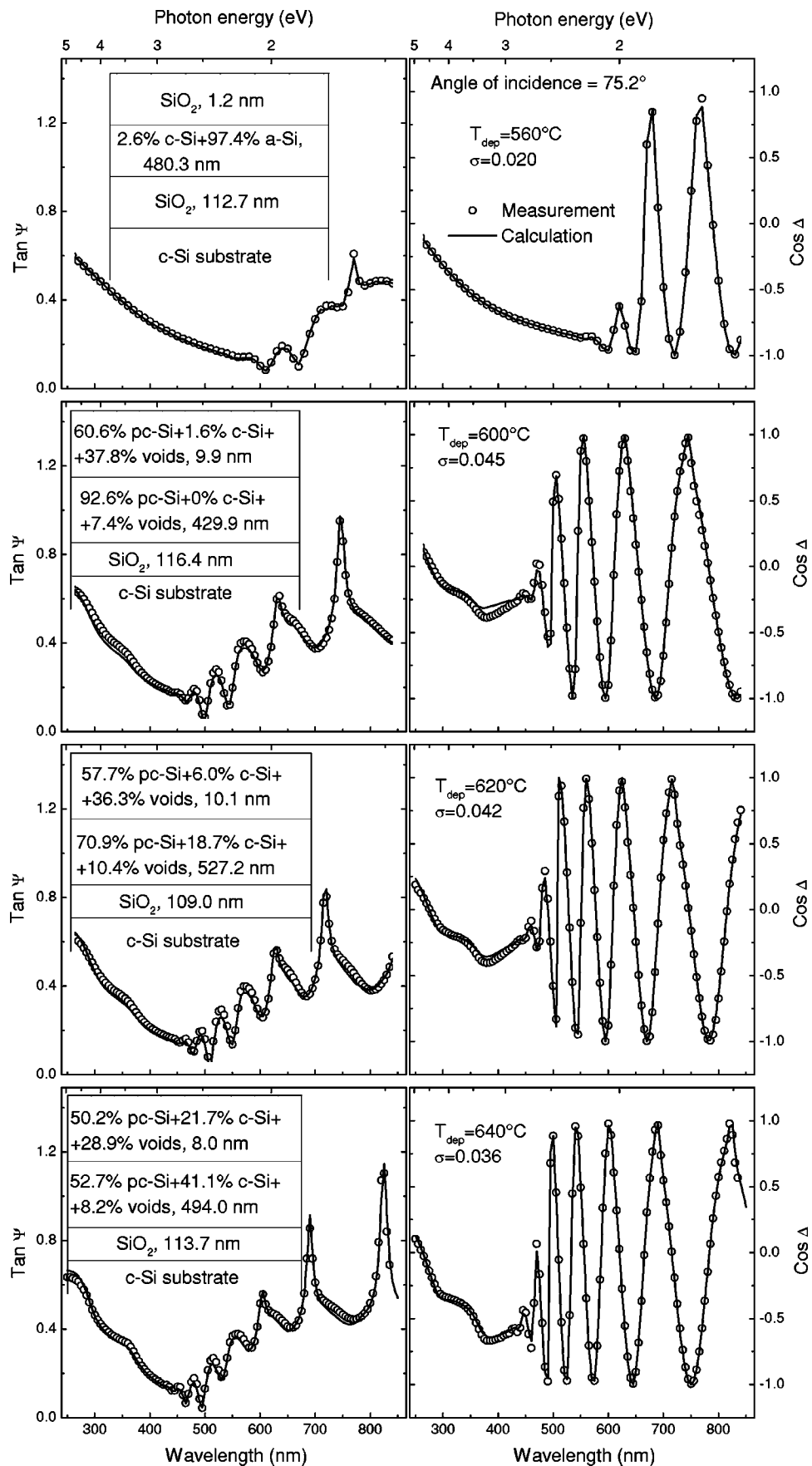


FIG. 2. Measured and fitted ellipsometry spectra on samples deposited at different temperatures. The optical models with the model parameters are shown in the inserts.

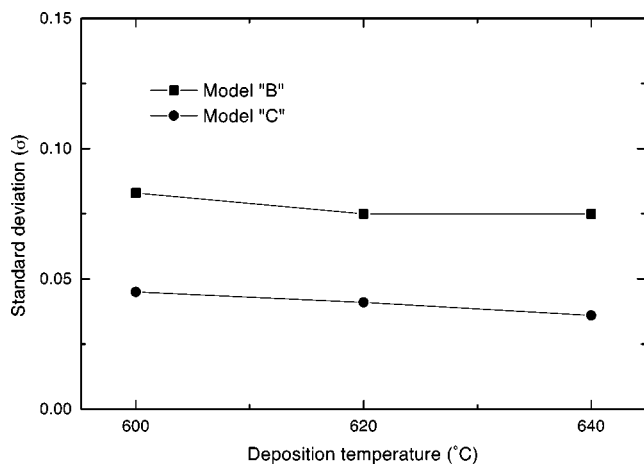


FIG. 3. Comparison of the σ values as a function of the deposition temperature using Model B and Model C of Fig. 1. The fitted curves for Model C are shown in Fig. 2.

electric functions of components “ a ” and “ b ,” and y is the screening parameter. The B-EMA is obtained with $y=2$ and $\bar{\epsilon}_h = \bar{\epsilon}$. The B-EMA has been proved to be the best model for the calculation of the dielectric function of polycrystalline silicon.^{32,33}

The dielectric function of LPCVD deposited polysilicon was previously modeled using a mixture of c -Si,³⁴ LPCVD a -Si,²⁸ and voids (Model B in Fig. 1). In the visible-near-UV range, the dominant contribution to the dielectric function ($\bar{\epsilon}$) comes from the electronic polarizability, which is determined by the kinds of atoms present, their bonding configurations, their density, and the presence or absence of long-range order. The amorphous silicon does not have a long-range order and shows only a single broad peak near 3.5 eV in the imaginary part of the dielectric function (ϵ_2).

In contrast, the crystalline silicon has a long-range order and shows two main sharp peaks near 3.4 eV (E_1 transition) and 4.2 eV (E_2 transition) in the ϵ_2 spectrum. The long-range order has a significant influence on both the line shape and magnitude of ϵ_2 . The c -Si and a -Si materials have no microstructure on the scale of 1 nm–1 μ m, that is, they are homogeneous on this scale. The pc -Si possesses inhomogeneity in this scale. When comparing the line shape of the fine-grained pc -Si (Ref. 28) to that of c -Si, the following features can be observed: there is a significant decrease in the amplitude of E_1 and E_2 peaks, and there is a shift of E_2 peak to lower energies. When the pc -Si reference spectra, regarded as a bulk sample, were fitted using the mixture of c -Si, a -Si, and voids, the LRA resulted in a mixture of 61.1% c -Si, 35.4% a -Si, and 3.5% voids. The low energy tail (below E_1) of pc -Si and the simulation agree well but there is a significant difference at the E_1 and E_2 regions. This result shows that the fine grained polycrystalline silicon cannot be described well with the mixture of c -Si, a -Si, and voids. A possible explanation is that the a -Si component may arise not from true amorphous inclusions but as a result of the model attempting to simulate the effect of grain boundaries in reducing the electron mean free path and broadening the peak structures. Size effects may also play an important role, i.e.,

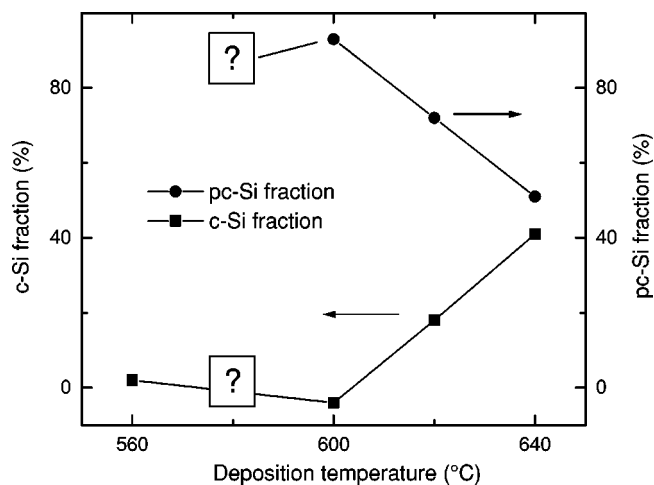


FIG. 4. c -Si and pc -Si fractions in polysilicon layers as functions of the deposition temperature. The question mark means that there was no reasonable fit obtained for the deposition temperature of 580 °C.

the crystalline inclusions are not large enough to preserve their own dielectric functions, or there is an increased number of grain boundaries, which cannot be described with the model “ c -Si+ a -Si+voids.” A comparison of the different models for the characterization of polysilicon structures has been published previously.³⁰

In this study, the dielectric function of pc -Si was described by the mixture of fine-grained pc -Si, c -Si, and voids (Model C in Fig. 1). Figure 2 shows the measured and fitted spectra together with the model parameters for samples deposited at different temperatures. The fit was also tried using the mixture of c -Si, a -Si, and voids (Model B in Fig. 1) again. Figure 3 shows that σ obtained using Model B is twice as large as in the case of Model C for the deposition temperatures of 600–640 °C.

The variation of the pc -Si and c -Si fractions in the polysilicon layers (see the inserts in Fig. 2) as a function of the deposition temperature is plotted in Fig. 4. At 560 °C, the layer is almost totally amorphous having 97% a -Si. The question marks mean that 580 °C is a transition temperature, at which our model cannot be used. There was no reasonable fit result obtained for the sample deposited at 580 °C (σ was 0.313 using Model C). A possible explanation is that its structure does not fulfill the above mentioned requirements for the effective medium approximation. This means that it cannot be considered as a microscopically heterogeneous but macroscopically homogeneous material which consists of a random mixture of separate phases with sizes between 1 nm and 1 μ m.

There is a linear increase in the c -Si fraction from 600 to 640 °C with a simultaneous decrease of the pc -Si fraction over the same range. It shows that the structure of the polysilicon layer deposited at lower temperature is closer to the fine-grained structure of the pc -Si reference data. The sharp decrease of the pc -Si fraction with increasing deposition temperature can be attributed to the change of the structure. It was shown earlier that the pc -Si reference data can be well applied for the modeling of different porous silicon structures.^{35–37} The similarity of porous silicon and polysili-

con is that both have small regions of *c*-Si embedded in voids (porous silicon) or in an amorphous matrix (polysilicon). *pc*-Si can be used in the optical models for both porous silicon and polysilicon, because it describes well the effect of the phase boundaries of small inclusions of single-crystalline regions on the dielectric function. The monotonic increase of the *c*-Si fraction in the polysilicon layer above 600 °C can be attributed to an increase of its grain sizes.

IV. MICROSCOPIC SURFACE ROUGHNESS

The microscopic surface roughness can be modelled with a density deficient overlayer.³² Our approach to study the effect of surface roughness is to replace the roughened “surface layer” by an equivalent homogeneous film, whose optical properties are determined from those of the substrate and ambient according to the EMA. This assumption can be used if the dimensions of the protrusions is less than the wavelength of the light. Then the light “sees” an average effective refractive index for the rough surface.

The directly obtained quantity from the optical model describing the surface roughness is its thickness. Whether this thickness is equal to the root-mean-square (rms) roughness, it can be determined by a comparison with AFM measurements. There are several comparative studies in the literature, where surface roughness was measured by SE and AFM. There is disagreement in the interpretation of the results. Liu *et al.*³⁸ wrote that “the rms values from AFM and the spectroscopic immersion ellipsometry (SIE) values are different with the SIE values yielding the larger R . The rms value should be about 1/2 the peak to valley height of protrusions. The after oxidation AFM and SIE measurements give this order and considering that the measurements are fundamentally different, with AFM being a local measurement, and ellipsometry averages the optical response of a relatively huge area, the agreement is gratifying.” This ratio shows significant discrepancies depending on the etching and oxidation times. Fang *et al.*¹⁰ emphasized that roughness measured by SE is not always equal to the RMS roughness measured by AFM. The ratio of the roughness measured by SE and AFM depends on the fast Fourier transformation (FFT) spectra of the surface. In contrast to Liu *et al.*, Suzuki and Adachi³⁹ measured the same roughness by AFM and SE with the comment that they are in “reasonable agreement” with each other.

To investigate this problem, surface roughness of polysilicon samples deposited at 620, 660, and 700 °C were measured by SE and AFM. Figure 5 shows the mean roughness (R_a) and rms roughness measured by AFM with scan window sizes of 1×1 , 10×10 , and $50 \times 50 \mu\text{m}^2$ correlated with the thickness of the top layer of SE representing the surface roughness. A virgin silicon reference sample covered with 2 nm native oxide layer was also measured by SE, and their data were evaluated with the same model as for the surface roughness layer (Model C) of the polysilicon samples. A layer thickness of 1.8 nm was obtained using this model. This point is also plotted in Fig. 5. The AFM roughness for the virgin silicon sample is 0.09 nm. If this point is considered to be the reference for zero roughness with a native

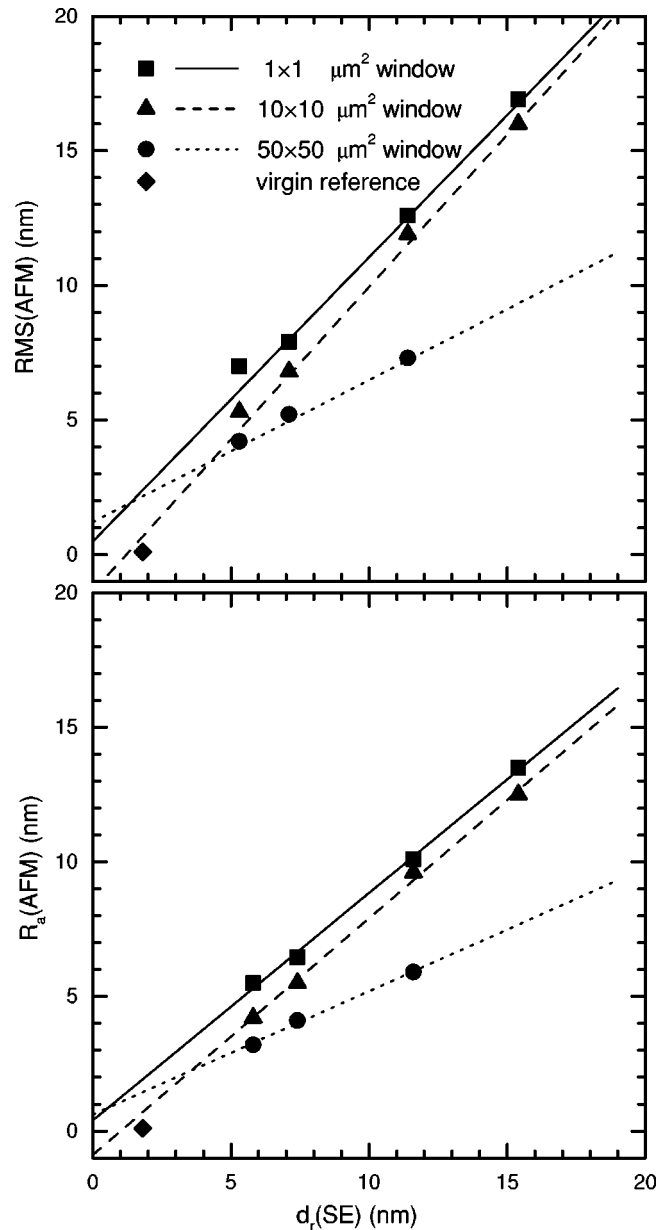


FIG. 5. Mean roughness (R_a) and root-mean-square (rms) roughness measured by AFM correlated with roughness determined by SE. $d_r(\text{SE})$ is the thickness of the top layer in the optical model representing the surface roughness.

oxide layer, then the origin of the plot in Fig. 5 has to be shifted to this reference point.

It is obvious from Fig. 5 that for both R_a and rms roughness a good correlation of the roughness determined by SE and AFM was obtained. We obtained average $d_r(\text{SE})/\text{rms}(\text{AFM})$ ratios of 0.89, 1.05, and 1.46, and average $d_r(\text{SE})/R_a(\text{AFM})$ ratios of 1.11, 1.31, and 1.85 using window sizes of 1×1 , 10×10 , and $50 \times 50 \mu\text{m}^2$, respectively, where d_r is the thickness of the modeled microscopic surface roughness. The results suggest that the interpretation of the $d_r(\text{SE})/\text{rms}(\text{AFM})$ or $d_r(\text{SE})/R_a(\text{AFM})$ ratio is not simple. This is because in addition to the window size effect, the tip geometry and/or the curvature or slope of the surface structures may influence the AFM results. SE is also affected by

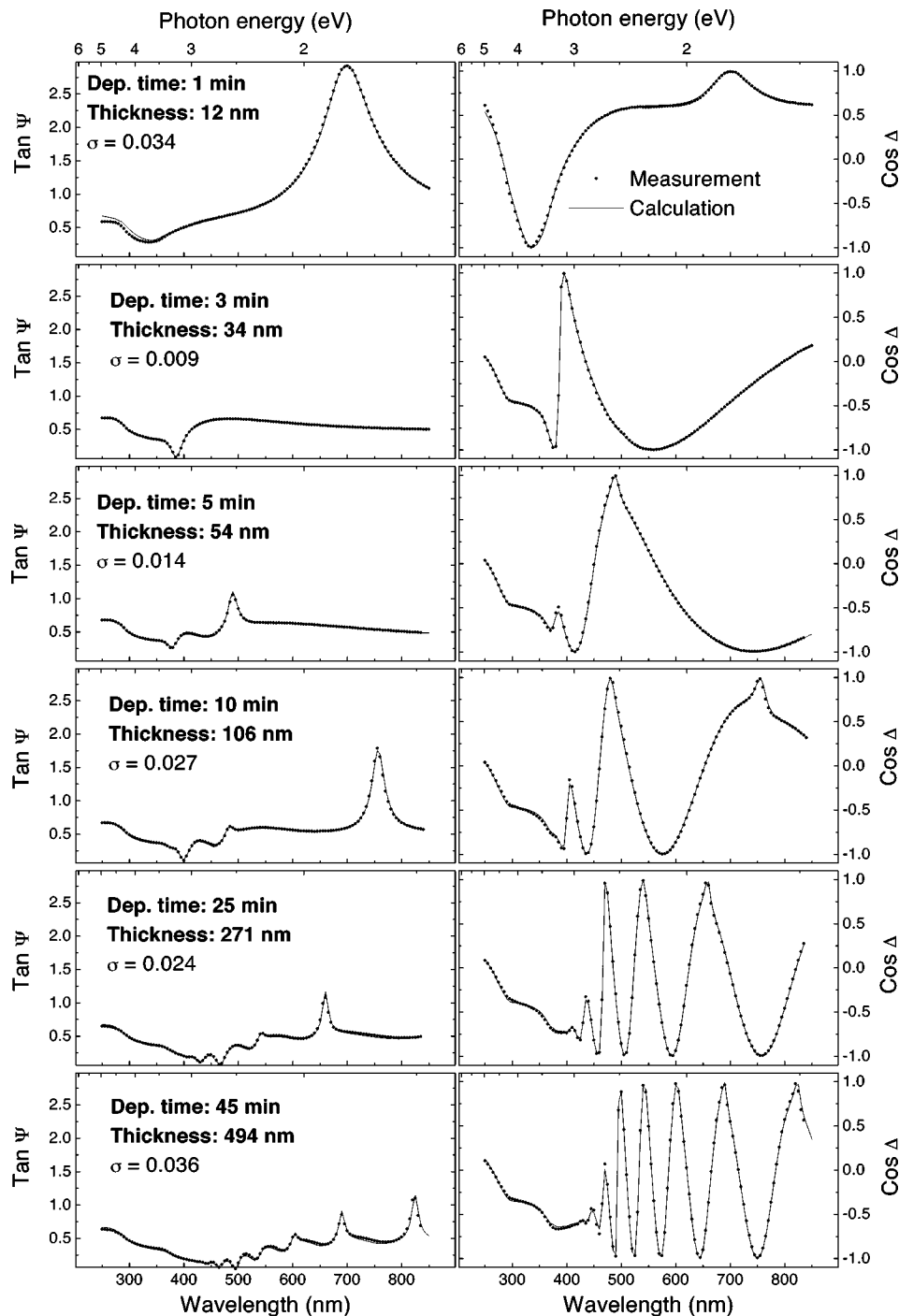


FIG. 6. Measured and fitted ellipsometry spectra for polysilicon samples deposited at 640 °C. The fitted model parameters are shown in Table I.

numerous factors such as the optical model used, the inhomogeneity or the FFT spectra of the surface profile (i.e., the surface geometry).¹⁰ The surface roughness can be characterized by the height of the protrusions, shape or density of surface features. These AFM and SE results characterize the surface roughness with only two values (roughness layer thickness and void fraction), which is not enough for the complete surface description. The rms roughness values were completed by the aid of fractal analysis⁴⁰ and FFT spectra were considered by several authors to obtain more information on the surface.^{10,41}

V. MODEL PARAMETERS VERSUS LAYER THICKNESS

Figure 6 shows the measured and the fitted spectra (with Model C) for polysilicon samples deposited at 640 °C with different layer thicknesses. The layer thickness of the samples ranges from 12 to 494 nm. The σ value is lower than 0.036 for all samples, which means a very good fit quality for all layers. The interference oscillations increasing with increasing layer thickness are clearly seen in the $\cos \Delta$ plot. The best fit model parameters for these samples are listed in Table I. The microscopic roughness changes from 3 to 8 nm,

TABLE I. Model parameters (Model C) obtained by the LRA for samples deposited at 640 °C. σ denotes the quality of the fit. The fitted curves are shown in Fig. 6

Polysilicon thickness (nm)	σ	Buried oxide thickness (nm)	Polysilicon layer					Roughness layer			
			thickness (nm)	<i>c</i> -Si (%)	<i>a</i> -Si (%)	voids (%)	<i>pc</i> -Si (%)	thickness (nm)	<i>c</i> -Si (%)	voids (%)	<i>pc</i> -Si (%)
12	0.034	115±1	12±0.3		9±2	51±0.5	40				
34	0.009	113±1	34±0.3	53±2		4±0.3	43	3±0.3	38±7	37±3	25
54	0.014	116±2	54±0.6	61±2		2±0.7	37	4±0.5	36±9	29±3	35
106	0.027	114±9	106±1.0	64±3		0±1.0	36	5.6±0.8	40±10	25±3	35
271	0.024	114±3	271±2.0	50±2		4±1.0	46	6.4±0.6	26±8	29±2	45
494	0.036	114±3	494±4.0	41±3		8±1.0	51	8±0.9	22±9	29±2	49

the thickness of the polysilicon layer changes from 12 to 494 nm, and the thickness of the buried oxide layer is about 115 nm. It has to be emphasized that the precision of the measurement of the buried oxide thickness is typically ± 3 nm or better even below a 494 nm polysilicon layer. The reasonably small confidence intervals, i.e., the low uncertainties, on Table I show that the precision of the determination of the model parameters is good.

Figure 7 shows the surface roughness and the volume fractions of voids in the roughness layer and in the polysilicon layer as a function of the thickness of the polysilicon layers deposited at 600, 620, and 640 °C. The thinnest polysilicon layers were modeled with only the roughness layer itself (*pc*-Si+*c*-Si+voids). The error bars on the figure represent the 95% confidence limits.

The curves describing the thickness and the void fraction of the surface roughness layer can be divided into two different regions. The region between the layer thicknesses of ~ 8 and 40 nm is characterized by a high surface roughness and a high void fraction. Both of them decrease rapidly with increasing layer thickness up to a layer thickness of 40 nm.

The increase of the thickness of the roughness layer with increasing thickness of the polysilicon layer above a thickness of 40 nm can be explained by the grains having larger dimensions on the surfaces of thicker layers.

The void fraction in the polysilicon layer has a thickness dependence similar to that of the roughness layer. It has a minimum close to 100 nm. For layers thicker than 100 nm, it increases and reaches 10% at a layer thickness of 600 nm.

In order to crosscheck the SE results, the void fraction of polysilicon layers (i.e., the density deficit) was independently determined by RBS (see Fig. 8 for selected samples). In each spectrum the region between the Si surface edge (channel No. 271) and the upper edge of the valley (channel Nos. 240, 236, and 228 in Fig. 8 for samples Nos. 4, 1, and 8, respectively) corresponds to the top polysilicon layer. The valley corresponds to silicon in the buried oxide, where the density of silicon decreases due to the presence of oxygen atoms. (The peaks below channel No. 140 correspond to the oxygen atoms.) The energy difference between helium ions scattered from the surface of the polysilicon layer and those scattered from the polysilicon-buried silicon dioxide interface is proportional to the number of silicon atoms in the polysilicon layer per square centimeter. The atomic density (atoms/cm³) of the layer is easy to determine by combination of RBS and

ellipsometry as shown in the case of buried, ion synthesized nitride,⁴² since RBS gives the areal density (atoms/cm²) and ellipsometry provides the layer thickness.

Having calculated the density of the top polysilicon layer (ρ_{poly} in atoms/cm³), the void fraction was determined as $(\rho_{\text{Si}} - \rho_{\text{poly}})/\rho_{\text{Si}}$, where ρ_{Si} is the density of the single-crystalline silicon. ρ_{poly} was calculated using the layer thickness obtained by SE. Void fraction values measured by SE and RBS are shown in Table II and are also plotted in Fig. 9 showing a good correlation between the SE and RBS results.

The σ values in Fig. 7 have a minimum at ~ 40 nm, which reveals that our model fits best to the structure of the initial phase of the deposition. Above 40 nm, σ slightly increases. The highest σ value is 0.056 for the thickest polysilicon layer deposited at 600 °C.

The dependence of the model parameters on the deposition temperature has the following feature: the void fraction in the roughness layer is higher for the lower deposition temperatures in the case of the thickest samples; similarly, there is a larger roughness layer thickness for the lower deposition temperatures above a layer thickness of ≈ 250 nm. It is also clear that in order to be able to compare the effect of the deposition temperature on the surface properties, layers with the same thickness have to be used to separate the influence of the layer thickness from that of the deposition temperature.

VI. CONCLUSIONS

The multilayer optical model based on using the B-EMA was used to describe properties of polysilicon layers having thicknesses ranging from 8 to 600 nm and deposited at temperatures between 560 and 640 °C. A better characterization of the polysilicon layer is achieved by using the reference data of a fine-grained *pc*-Si silicon in the optical model.

The dependence of the optical model parameters on the layer thickness and deposition temperature have been investigated. The linear increase of the *c*-Si fraction and the simultaneous decrease of the *pc*-Si fraction in the polysilicon layer with increasing deposition temperature are observed. At lower deposition temperatures (near 600 °C), the deposited layer is closer to the fine-grained structure. At higher deposition temperatures (at 640 °C and above), the increased *c*-Si fraction may correspond to the increasing *c*-Si grain size.

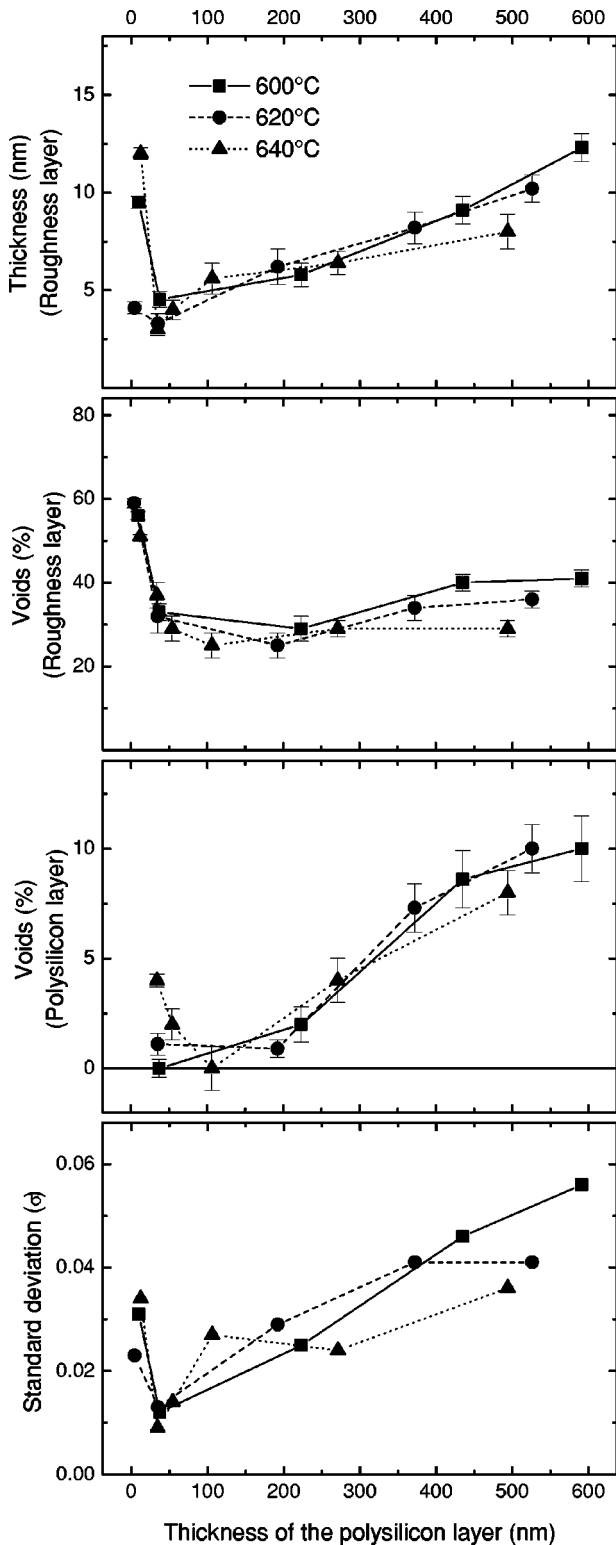


FIG. 7. Model parameters and σ values as functions of the layer thickness for polysilicon samples deposited at different temperatures.

It has been shown that independently of the AFM window sizes, good correlation of the surface roughness determined by SE and AFM was obtained. Average $d_r(\text{SE})/\text{rms}(\text{AFM})$ ratios of 0.89, 1.05, and 1.46, and average $d_r(\text{SE})/R_a(\text{AFM})$ ratios of 1.11, 1.31, and 1.85 for AFM window sizes of 1×1 , 10×10 , and $50 \times 50 \mu\text{m}^2$, respectively are obtained. The interpretation of the $d_r(\text{SE})/\text{rms}(\text{AFM})$ or

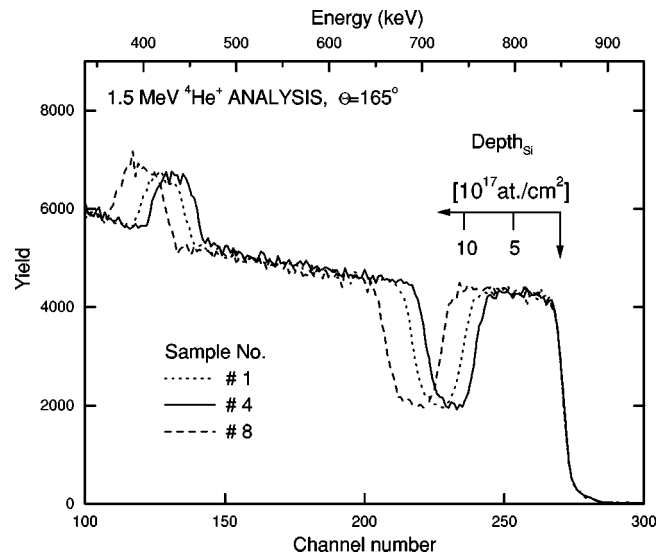


FIG. 8. RBS spectrum of three different polysilicon samples. Details of the deposition conditions are given in Table II.

$d_r(\text{SE})/R_a(\text{AFM})$ ratio is not simple. In addition to the window size effect, the tip geometry or the curvature or slope of the surface structures may influence the AFM results.

The dependence of the optical model parameters on the layer thickness distinguishes the stages of the layer growth. The region below a polysilicon layer thickness of 40 nm is characterized by a large roughness layer thickness and high void fraction in the roughness layer representing the first stage of the layer growth. There is a considerable increase in roughness layer thickness and void fraction in the polysilicon layer with increasing layer thickness. The amount of voids in the polysilicon layer was determined independently by RBS, and a good correlation between RBS and SE results was obtained.

The optical models used here provide a better understanding of the structural change of the polysilicon layers as a function of deposition time and temperature. Because the structure of the *pc*-Si changes with changing deposition condition, the adopted layer-structure models and reference dielectric-function data have to be paid attention.

TABLE II. Comparison of the void fraction of polysilicon samples deposited varying the deposition temperature and the deposition time, measured by SE and RBS.

Sample No.	Deposition time (min)	Deposition temperature (°C)	Void fraction	
			spectroscopic ellipsometry (%)	RBS (%)
1	42	600	2±0.8	5.8±2.5
2	75	600	8.6±1.3	10.4±1.9
3	100	600	10±1.5	11.4±1.8
4	25	620	0.9±0.6	3.2±3.1
5	45	620	7.3±1.1	8.6±1.9
6	60	620	10±1.1	11.0±1.7
7	10	640	0±1.0	1.8±2.9
8	25	640	4±1.0	5.6±2.2
9	45	640	8±1.0	9.4±1.6

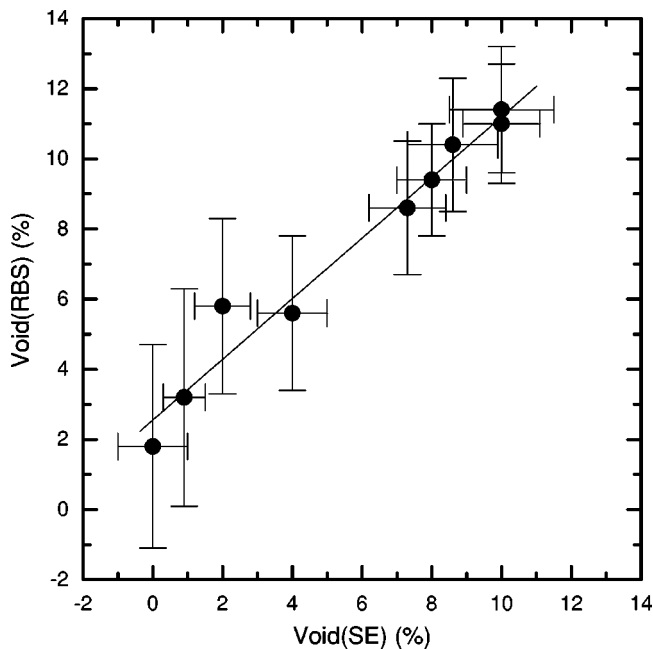


FIG. 9. Correlation of the void fraction values measured by SE and RBS for polysilicon samples shown in Table II.

ACKNOWLEDGMENTS

Measurements and sample preparation were carried out at the Fraunhofer-Institut für Integrierte Schaltungen in Erlangen, Germany. Support of the Volkswagen Stiftung (AOST Nr. 814 328-1) and from OTKA Grants Nos. T025928 and T030441 is greatly appreciated.

- ¹I-W. Wu, A. Chiang, M. Fuse, L. Öveçoglu, and T. Y. Huang, *Mater. Res. Soc. Symp. Proc.* **182**, 107 (1990).
- ²S. J. N. Mitchell, D. W. McNeill, S. H. Raza, B. M. Armstrong, and H. S. Gamble, *Mater. Res. Soc. Symp. Proc.* **182**, 35 (1990).
- ³D. Meakin, J. Stoemenos, P. Migliorato, and N. A. Economou, *J. Appl. Phys.* **61**, 5031 (1987).
- ⁴T. I. Kamins, M. M. Mandurah, and K. C. Saraswat, *J. Electrochem. Soc.* **125**, 927 (1978).
- ⁵E. Ibok and S. Garg, *J. Electrochem. Soc.* **140**, 2927 (1993).
- ⁶I. An, Y. Cong, N. V. Nguyen, B. S. Pudliner, and R. W. Collins, *Thin Solid Films* **206**, 300 (1991).
- ⁷R. W. Collins, I. An, H. V. Nguyen, and Y. Lu, *Thin Solid Films* **233**, 244 (1993).
- ⁸W. Lehnert, R. Berger, C. Schneider, L. Pfitzner, H. Ryssel, J. L. Stehle, J.-P. Piel, and W. Neumann, *Thin Solid Films* **313–314**, 255 (1998).
- ⁹W. Lehnert, P. Petrik, C. Schneider, L. Pfitzner, and H. Ryssel, *ULSI Conference*, Gaithersburg NIST, [AIP, Conf. Proc. **443** 326 1998].

- ¹⁰S. J. Fang, W. Chen, T. Yamanaka, and C. R. Helms, *Appl. Phys. Lett.* **68**, 2837 (1996).
- ¹¹C. Fluerau, M. Gartner, C. Rotaru, D. Dascalu, G. Andriescu, and P. Cosmin, *Microelectron. Eng.* **31**, 309 (1996).
- ¹²P. Petrik, L. P. Biró, M. Fried, T. Lohner, R. Berger, C. Schneider, J. Gyulai, and H. Ryssel, *Thin Solid Films* **315**, 186 (1998).
- ¹³D. E. Aspnes, A. A. Studna, and E. Kinsbron, *Phys. Rev. B* **29**, 768 (1984).
- ¹⁴S. Logothetidis, *J. Appl. Phys.* **65**, 2416 (1989).
- ¹⁵S. Logothetidis, H. M. Polatoglou, and S. Ves, *Solid State Commun.* **68**, 1075 (1988).
- ¹⁶D. E. Aspnes, *Thin Solid Films* **89**, 249 (1982).
- ¹⁷M. Fried, T. Lohner, J. M. M. de Nijs, A. van Silfhout, L. J. Hanekamp, Z. Laczik, N. Q. Khánh, and J. Gyulai, *J. Appl. Phys.* **66**, 5052 (1989).
- ¹⁸T. Lohner, W. Skorupa, M. Fried, K. Vedam, N. Nguyen, R. Groetzschel, H. Bartsch, and J. Gyulai, *Mater. Sci. Eng., B* **12**, 177 (1992).
- ¹⁹J. Vanhellemont, H. E. Maes, and A. de Veirman, *J. Appl. Phys.* **65**, 4454 (1989).
- ²⁰K. Vedam, P. J. McMarr, and J. Narayan, *Appl. Phys. Lett.* **47**, 339 (1985).
- ²¹Y. M. Xiong, P. G. Snyder, J. A. Woollam, E. R. Krosche, and Y. Strausser, *Mater. Res. Soc. Symp. Proc.* **182**, 219 (1990).
- ²²T. Lohner, M. Fried, J. Gyulai, K. Vedam, N. V. Nguyen, L. J. Hanekamp, and A. van Silfhout, *Thin Solid Films* **233**, 117 (1993).
- ²³M. Fried, T. Lohner, W. A. M. Aarmink, L. J. Hanekamp, and A. van Silfhout, *J. Appl. Phys.* **71**, 2835 (1992).
- ²⁴L. M. Asinovsky, *Thin Solid Films* **233**, 210 (1993).
- ²⁵B. G. Bagley, D. E. Aspnes, A. C. Adams, and C. J. Mogab, *Appl. Phys. Lett.* **38**, 56 (1981).
- ²⁶P. G. Snyder, Y.-M. Xiong, and J. A. Woollam, *Surf. Interface Anal.* **18**, 113 (1992).
- ²⁷C. Fluerau, M. Gartner, D. Dascalu, and C. Rotaru, *J. Phys. III* **6**, 225 (1996).
- ²⁸G. E. Jellison, Jr., M. F. Chisholm, and S. M. Gorbalkin, *Appl. Phys. Lett.* **62**, 3348 (1993).
- ²⁹T. Suzuki and S. Adachi, *Jpn. J. Appl. Phys., Part 1* **32**, 4900 (1993).
- ³⁰P. Petrik, M. Fried, T. Lohner, R. Berger, L. P. Biró, C. Schneider, J. Gyulai, and H. Ryssel, *Thin Solid Films* **313–314**, 259 (1998).
- ³¹E. Kótai, *Nucl. Instrum. Methods Phys. Res. B* **85**, 588 (1994).
- ³²D. E. Aspnes, J. B. Thettn, and F. Hottier, *Phys. Rev. B* **20**, 3292 (1979).
- ³³D. E. Aspnes, *Proc. SPIE* **276**, 312 (1981).
- ³⁴*Handbook of Optical Constants of Solids*, edited by E. D. Palik (Academic, New York, 1985).
- ³⁵M. Fried, H. Wormeester, E. Zoethout, T. Lohner, O. Polgár, and I. Bársony, *Thin Solid Films* **313–314**, 459 (1998).
- ³⁶T. Lohner, N. Q. Khánh, and Zs. Zolnai, *Acta Phys. Slov.* **48**, 441 (1998).
- ³⁷I. Bársony, J. G. E. Klappe, and É. Vázsonyi, T. Lohner, and M. Fried, *Mater. Res. Soc. Symp. Proc.* **342**, 91 (1994).
- ³⁸Q. Liu, J. F. Wall, and E. A. Irene, *J. Vac. Sci. Technol. A* **12**, 2625 (1994).
- ³⁹T. Suzuki and S. Adachi, *Jpn. J. Appl. Phys., Part 1* **33**, 5600 (1994).
- ⁴⁰L. Spanos, Q. Liu, and E. A. Irene, *J. Vac. Sci. Technol. A* **12**, 2653 (1994).
- ⁴¹Q. Liu, L. Spanos, C. Zhao, and E. A. Irene, *J. Vac. Sci. Technol. A* **13**, 1977 (1995).
- ⁴²N. Q. Khánh, M. Fried, G. Battistig, Z. Laczik, T. Lohner, E. Járóli, V. Schiller, and J. Gyulai, *Phys. Status Solidi A* **108**, K35 (1988).